# EEG Simulation: Variation of Spectral Envelope, Pulse Synchrony and ≈40 Hz Oscillation.

J.J.Wright*

June 1996,
Revised October 1996.

**Abstract**

**Macroscopic EEG travelling wave phenomena and cortical pulse synchronisation effects are related within a single simple simulation. Nonspecific activation acts to control the transfer function of the simulated cortex, and thus determines the relative amplitude of macroscopic EEG waves generated by rhythmic inputs.When concurrent asynchronous excitatory inputs to separate, local, cortical sites are introduced, the simulation reproduces both gamma band (40Hz) ECoG activity and synchronous oscillation of action potential pulse density at the seperate sites. The gamma band ECoG and pulse synchrony effects depend on different mechanisms - the former upon local excitatory/inhibitory interactions, and the latter on cortico-cortical interactions. The pattern of synchronous activity depends upon both structural and dynamic aspects of gain, and is sustained by linearised versions of the simulations state-equations. Dynamic properties of the simulation which are independent of scale, describe both microscopic and macroscopic phenomena, all in accord with physiological findings (Singer and Gray 1995).**

*Mental Health Resarch Institute of Victoria. email. - jjw@cortex.mhri.edu.au ; tel. - 61 39388 1633; fax. - 61 3 9387 5061 ; Corresp.- author at MHRI, Locked Bag 11, Parkville, Victoria 3052, Australia.

## 1. Introduction.

*1.1. ECoG elementary properties.*

The dendrites of cortical pyramidal neurones generate local field potentials (LFP) during processing of cognitive information (John et al 1969; Mitzdorf 1988; Gevins et al 1983;Picton and Hillyard 1988). Summed at a point on the cortical surface these LFP form the ECoG., and when recorded via the scalp, the electroencephalogram (EEG). The terms EEG, ECoG and LFP can be treated as interchangable, if the relative degree of spatial and temporal filtering of the underlying cortical events is kept in mind. The fluctuating surface potentials appear, in general, to be associated with, and arise from, travelling waves of local potential, which thus reflect waves of mean local dendritic potential (Thatcher et al 1966; Burkitt 1986).

In EEG certain spectral characteristics are commonly observed (eg Walter et al 1967). These include the alpha, beta and gamma rhythms, and "desynchronisation", which appears at high levels of alertness. Desynchronised ECoG typically yields a power spectrum without prominent peaks, loosely describable as a "1/f" spectrum (Freeman 1991).

The roles played by cortical and subcortical systems in generating and regulating the EEG are partially understood. Both slow-time-scale diffuse regulation of excitatory and inhibitory tone to the cortex, and the injection of rhythmic activities are involved. Inherently rhythmic neurones and resonances within the cerebrum may also play a part (Steriade et al 1990).

*1.2 LFP and action potential relations.*

Recently (Eckhorn et al 1988; Gray and Singer 1989; Gray et al 1989, Singer 1994) it has been shown that multiunit action potentials at simultaneously stimulated sites in the cortex and elsewhere in the brain can exhibit synchronous fluctuations of pulse density. Typically these results are obtained when retinal sites are activated selectively by moving bars. Concurrently, the LFP in the neighbourhood of the synchronous pulse activity often, but not invariably, oscillates in the gamma band (around 40Hz, varying from about 30-80Hz). These findings have been recently reviewed by Singer and Gray (1995). They show that synchrony between concurrently active cortical sites is typically at zero time lag, and is manifested at several scales - intracolumnar, intercolumnar and interareal. Both structural connectivity (eg, by cortico-cortical fibres crossing the corpus callosum) and functional dynamic state (eg cortical visual areas respectively specific for colour and

form, responding to a particular colour/form combination) determines the regions which enter synchrony with each other. In most instances these results cannot be explained by synchronous concurrent inputs to the seperate sites.

Although synchrony appears in most instances at zero lag, lag relations between stimulated sites are somewhat more complicated. For instance, cortical neurones driven by optimal stimuli appear to lead other neurones in the neighbourhood which are suboptimally stimulated, by a few milliseconds (Konig et al 1995). It appears possible that synchrony may play a part in spatiotemporal association and segmentation of the perceptual field, and thus resolve the "binding" problem (Singer and Gray 1995).

No simulation or other general explanation has been advanced to relate macroscopic EEG phenomena (which involve lagged relations between events at different cortical areas) with local, zero lag, pulse and LFP synchrony and oscillation.

*1.3 Previous simulation and explanatory findings.*

Freeman (Freeman 1975, 1990, 1991, 1995) and Nunez (1981, 1989, 1995) have developed models for EEG which respectively emphasise micro/mesoscopic and macroscopic waves. The Freeman and Nunez approaches may be compatable ( Wright 1990; Wright and Liley 1996) despite their emphasis on nonlinear versus linear mechanisms.

A number of simulations deal specifically with synchronous oscillation about 40Hz. Whittington et al (1995) have produced a detailed cellular model for hippocampal cells, which accounts for the oscillation as arising from activation of inhibitory cells depending upon fast ($GABA_A$) receptors, and have further generalised this approach to the cortex (Traub et al 1996). Alternate explanations depend on intrinsic oscillations in stellate and pyramidal cells (Llinas et al 1991) and in thalamocortical projections (Steriade et al 1993). For the olfactory cortex at least, feedback interactions between excitatory and inhibitory cells impose an approximately 40Hz oscillation, as evidenced in spectral and unit phase recordings (Bressler and Freeman 1980, Eeckman and Freeman 1990).

It has also been shown in simulation that local lateral inhibition might entrain synchronous oscillations (Nischwitz and Glunder 1995), that limit cycle oscillators representing single neurones can entrain to several independent synchronised clusters (Tass and Haken 1996), and that non-oscillating

cells in Synfire chains can shift phase into synchrony (Arnoldi and Brauer 1996).

*1.4. Basis for the present study.*

In Wright and Liley (1995) a simple simulation of EEG in cat and human was reported, which was shown able to reproduce peak spectral densities about the range of the major cerebral rhythms, a "shift to the right" (ie, increasing high frequency power) with increasing nonspecific cortical excitation, travelling waves with velocities close to experimental measures (Lopes da Silva and Storm van Leeuwen 1978; Thatcher et al 1986; Wright and Sergejew 1991; Burkitt 1994) emmanating from localised inputs, and frequency/wavenumber characteristics similar to that of real ECoG. (The last result marred by unavoidable problems of spatial aliasing).

The same simulation methods have been applied in the present paper, firstly to clarify the spectral and travelling wave characteristics, secondly to reproduce conditions and results concerned with synchrony and oscillation analogous to experiments conducted by Singer and Gray and others, and thirdly to elucidate the dependence of the findings on particular physical mechanisms.

By these means it is aimed to show that a unified explanation of both zero lag synchrony and travelling wave phenomena can be advanced, and that the mechanisms for these effects need not depend upon nonlinear phase-locking, complicated synaptodendritic dynamics, or synchrony of cortical inputs. First steps have also been taken to show that certain properties of synchrony are scale invariant and may apply to interactions among individual cells, or interacting populations.

**2. Methods.**

*2.1. An Outline of Single-layered Cat Cortex ECoG Simulation - Wright and Liley (1995).*

Elements of connectivity in the simulation are sketched in Diagram 1.

*2.1.1. Unit Volume, Pulse Density and Local field Potential.*

For the $N$ cells in unit volume, pulse density, $Q$, is given by

$$Q = \frac{1}{N} \sum_{i=1}^{N} q_i \qquad (1)$$

where $\{q_i\}$ are the states of the cells, and $q_i = 0$ or 1,depending on whether the individual cell is sub- or suprathreshold.

The local field potential, $V$, and $Q$ are related by

$$Q = (1 + e^{a(V-3)})^{-1} \qquad (2)$$

which represents sigmoidal response of pulse density with respect to $V$, consequent to the Gaussian distribution of action potential thresholds with respect to $V$. Voltage units are standard deviations (SD) of the distribution of cell thresholds, and the distribution is considered truncated at 3 SD from the mean threshold.

Parameter a has the value -1.82, rather than the conventional $-\sqrt{2}$ as this choice produces somewhat better approximation over the usual low pulse density operating range of the simulation.

*2.1.2. Synaptic Density as a measure of Coupling strength.*

Within and between unit volumes, the strength of synaptic coupling between any two masses of cells of uniform type, or the recurrent coupling of any one mass to itself, was treated as proportional to the synaptic density of the appropriate type, expressed as a fraction of the total synapses in unit volume. The nomenclature adopted reflects Braitenberg and Shuz's (1991) association of apical and basal dendritic systems with cortico-cortical ($\alpha$-type) and intracortical ($\beta$-type) axo-synaptic connections. Subscripts, $ei$ for example, indicate that the synaptic class is that of excitatory cells afferent to inhibitory cells and so on. The relevant types of synaptic density are then:

* $\alpha_{ei}, \alpha_{ee}$ . Synaptic densities associated with the entirely excitatory cortico-cortical fibres. For a typical unit volume at cortical coordinates $(0, 0)$, partial densities can be defined by their origins from surrounding volumes at $(x, y)$ as $\alpha_{ee}(x, y)$

For cat cortex, $\alpha_{ee} = 0.765$, $\alpha_{ei} = 0.1$.

* $\beta_{ee}, \beta_{ei}, \beta_{ie}, \beta_{ii}$. Synaptic densities of intracortical connections.

$\beta_{ee}$= 0.0845, $\beta_{ei} = 0.00149$, $\beta_{ie}$= 0.0228, $\beta_{ii} = 0.004$.

* $\mu_{ee}, \mu_{ei}$. Synaptic densities of nonspecific cortical afferents. A maximally conservative estimate for density of non-specific inputs to cortex was made - namely that only 1% of synapses are of this origin.

$\mu_{ee} = 0.0077$, $\mu_{ei} = 0.0011$.

* $M_{ee}$, the density associated with specific cortical afferents - a value which was not required for purposes of simulation.

Calculations of synaptic density were made by methods reported in Liley and Wright (1994) and Wright and Liley (1995). We have since revised these estimates somewhat, but for ease of comparison with earlier work, the earlier

values are retained here. (The spectral and other properties of the simulation are little effected by change to the later values.)

*2.1.3. Dendritic Delay (pulse/wave conversion), Synaptic Gain and Axonal Delay*

System delays imposed by lag time of transmission through the cortical dendrites was modelled in a simplified form based on the findings of Freeman (1991).

Thus where $g$ is a measure of synaptic gain, $Q_a$ is the afferent pulse action density, $\{w_j\}$ are discretised lag weights approximating the rise and fall of dendritic potential in response to a unit-amplitude pulse input, and $\Delta t$ is the discrete time step (0.1ms), then the time response of local field potential is given by

$$V(t) = g \sum_{j=1}^{n} w_j Q_a(t - j\Delta t) \qquad (3)$$

The $\{w_j\}$, $j = 1...n$, were in the form of an isosceles triangular function, with maximum at $j = n/2$ being the 5ms lag weight. For $j = 1$ and $n$, $w_j = 0$, and $\sum^{n} w_j = 1$.

The synaptic gain, $g = 37$ units, where each unit is an SD of threshold distribution.

Axonal delays corresponded to a uniform velocity of conduction of 9 m/sec, matching physiological average estimates (Nunez 1995) Within each unit volume axonal conduction lags were treated as zero. Delays of conduction between unit volumes were calculated from $\Delta\tau = r_{pq}/\nu$, where $\Delta\tau$ is axonal conduction lag over the Euclidean distance $r_{pq}$ between the $p$th unit volume and the $q$th unit volume and axonal conduction velocity is $\nu$.

*2.1.4. Coupling of unit volumes to simulate extended cortex.*

An extended area of cortex was simulated by unit volumes in a 20 X 20 matrix, each volume connected with its neighbours so that the coupling strengths, $\alpha_{ee}(x, y)$ declined with $r_{pq}$ as a Gaussian function with standard deviation of 4 distance units,where a distance unit was the side of one cell of the 20 X 20 matrix. This approximates to distribution of cortico-cortical fibres in the cat brain if the distance unit is taken as about 0.9 mm, giving an axonal delay of 0.1 ms/distance unit.

Boundary conditions were toroidal, conveniently imposing a closed condition.

*2.1.5. State Transition Equations*

Defining $V_{e(p)}, V_{i(p)}, Q_{e(p)}, Q_{i(p)}$, as the $p$th unit volume's state variables, at time $t$,

$$Q_{e(p)} = (1 + e^{a(V_{e(p)}-3)})^{-1}, \quad Q_{i(p)} = (1 + e^{a(V_{i(p)}-3)})^{-1} \qquad (4)$$

$$V_{e(p)} = g \sum_{j=1}^{n} w_j Q_{ae(p)}(t - j\Delta t), \;\; V_{i(p)} = g \sum_{j=1}^{n} w_j Q_{ai(p)}(t - j\Delta t) \quad (4a)$$

where $Q_{ae(p)}, Q_{ai(p)}$ are afferent synaptic action densities for the $p$th unit volume, receiving cortico-cortical inputs from $q$ unit volumes, $q = 1...u$.

$$Q_{ae(p)} = \beta_{ee} Q_{e(p)} - \beta_{ie} Q_{i(p)} + M_{ee} Q_{s(p)} + \mu_{ee} Q_{ns(p)} + \sum_{1}^{u} \alpha_{ee}(r_{pq}) Q_{e(q)}(t - r_{pq}/\nu)$$

$$Q_{ai(p)} = \beta_{ei} Q_{e(p)} - \beta_{ii} Q_{i(p)} + M_{ei} Q_{s(p)} + \mu_{ei} Q_{ns(p)} + \sum_{1}^{u} \alpha_{ei}(r_{pq}) Q_{e(q)}(t - r_{pq}/\nu)$$

(5) and (5a)

Consequent to the symmetry of long range couplings, $\sum_{1}^{u} \alpha_{ee}(r_{pq}) = \alpha_{ee}$ and $\sum_{1}^{u} \alpha_{ei} = \alpha_{ei}$.

*2.2 Inputs and Control Parameters.*

*2.2.1 Definitions, and operating ranges.*

System inputs as defined in eqns (5) are $Q_s$ and $Q_{ns}$.

$Q_s$ was delivered as a zero mean Gaussian white noise (Marsaglia and Zaman 1987) added to the value of $Q_e$ in selected unit volumes. The standard deviation of the white noise was limited so that $Q_e$ in the input unit volumes never became negative. This input could be used to introduce time-varying inputs to selected sites, mimicking special sensory input.

$Q_{ns}$ was delivered at constant positive values to each unit volume during each simulation run, thus acting as a control parameter operating in the mean excitatory range. Applied to all unit volumes, it is analogous to non-specific cortical excitation as delivered by the reticular formation. When $Q_{ns}$ is supplied selectively to particular unit volumes in association with $Q_s$ it acquires additional analogy to the mean excitatory tone associated with

the specific sensory input, since the end result in the simulation is the same. The latter usage also justifies the use of values for selective $Q_{ns}$ inputs greater than 1, although the definition of pulse density limits $\{Q\}$ to the range 0 - 1. Two further reasons justify this liberal range of $Q_{ns}$. Firstly, $\mu_{ee}, \mu_{ei}$ (the nonspecific synaptic densities) have been very conservatively estimated in our anatomical estimates (Liley and Wright 1994). Secondly, since cortical nonspecific activation depends upon relatively long-acting neuromodulators, this increases the effective nonspecific pulse density.

*2.2.1. Positions and durations of inputs.*

Inputs to the simulation were organised in two ways:

(1) To allow travelling waves to be studied in simplified conditions, $Q_{ns}$ inputs were delivered uniformly to all unit volumes in the matrix, and $Q_s$ was delivered to the excitatory cell compartment of the unit volumes in the zeroeth column of the matrix.

(2) To allow the effects of conjoint excitation and driving of localised cortical sites to be studied, $Q_{ns}$ was set to 0.1 for all unit volumes except two. The two excited sites were then delivered higher $Q_{ns}$ inputs, and (usually) asynchronous $Q_s$ inputs - ie, noise sequences generated from different seed values.

White noise and sinusoidal forms of $Q_s$ were utilised as detailed with specific results.

Unless specifically stated, all simulation runs began with 0.8s of both $Q_s$ and $Q_{ns}$ input, beginning with $\{Q_e, Q_i\}$ all zero at $t$ = zero. Outputs were then analysed over the subsequent 0.8 - 1.6s epoch.

*2.3 Outputs.*

These were the time series of $\{V_e, Q_e\}$. Selected members of $\{V_e(t)\}$ underwent spectral analysis by Fast Fourier Transform, and pairs of $\{Q_e(t)\}$ were used to obtain Pearson's correlation coefficient as a function of lag, between selected sites.Ensemble averages for each of these measures were constructed by averaging the results obtained from the 0.8s individual runs, usually over 100 samples, or as indicated with specific results.

*2.4. Specialised forms of the simulation's state equations.*

*2.4.1 Linearised model form.*

To determine dependence of the simulation's dynamics upon nonlinear effects, it was useful to apply a linearised version of the state equations and

contrast the results in runs of this type with runs generated using equations (4&5).

Differentiating equation (2),

$$dQ/dV = -ae^{a(V-3)}(1+e^{a(V-3)})^{-2} \qquad (6)$$

and thus for any given mean value,$V_o$ of $V$

$$Q = \{dQ/dV_{V=V_o}\} * (V - V_o) \qquad (6a)$$

is a linearised approximation of (2), which can be generalised to eqns (4&5). The mean values of $\{V_e, V_i\}$ obtained from the standard, nonlinear, simulation at steady-state, were thus the required $\{V_o\}$ to operate the simulation with equivalent gains to the standard condition, but without other nonlinear signal transformations.

*2.4.2 Roles of intracortical and cortico-cortical interactions.*

To study the roles played by different classes of synaptic coupling, special simulations were performed in which all couplings of the sets $\{\alpha_{ee}\}$, $\{\beta_{ee}\}$, $\{\beta_{ie}\}$,and $\{\beta_{ii}\}$ were set to zero, alone or in combinations. Results were contrasted with matched standard simulation runs.

*2.4.3 Effects of cortico-cortical coupling symmetry.*

To enable the consequences of a rich variety of asymmetrical coupling conditions to be studied by variation of a single parameter, the strength of $\alpha$-type couplings between any two unit volumes, a function of distance of seperation, $r_{pq}$, was eliptically reweighted according to $r_{pq} \rightarrow \sqrt{x^2 + (Ey)^2}$, where $x$ and $y$ are the distances of seperation along the rows and columns of the unit volumes. $E$ is equal to 1 for the usual 2-D gaussian distribution of connections. For $E \neq 1$, the total input connectivities per unit volume were summed and normalised so that the total input synaptic density remained equal to $\alpha_{ee}, \alpha_{ei}$. Adjacent unit volumes were assigned reciprocal values of $E$ alternately along any row, column and diagonal on the matrix, thus generating asymmetry of coupling between most unit volumes. Results of simulations generated for a variety of values of $E$, were again contrasted with matched standard simulations.

*2.4.4 Simulation of events at different scales.*

The state equations have a form which is applicable independent of scale provided that at very small scales the synaptic densities attributed to intracortical and cortico-cortical connections, and axonal delays are appropriately

corrected. This property arises since $N$, the number of cells per unit volume is arbitrary. Voltage units are defined in standard deviations of cell threshold, and the sigmoidal nonlinearity can be interpreted as reflecting either the distribution of thresholds of individual cells or the probability that single cells will fire at a given level of dendritic depolarisation.. Whereas toroidal bounds are most appropriate for the simulation of whole brain-scale events, for small scale events zero boundary conditions best reflect the connectivity of a small locale of cells, considered as embedded in the larger cerebral cortex.[1].Details are discussed further in 3.2.3

## 3. Results.

*3.1. System Properties with uniform Qns inputs - Travelling waves associated with low pulse densities.*

Figure 1 shows ensemble average spectral properties of simulated ECoG. The driving noise, $Q_s$, was input synchronously (ie, the identical time series) to each element in the zeroeth column of the matrix, and in each graph the ECoG power spectrum from the unit volume at the 10th column and row of the matrix is displayed, as representative of spectra from across the matrix. As described in Wright and Liley (1995) these spectra reflect travelling wave activity in the matrix, generated by the $Q_s$ input. Within each graph, spectra are shown for progressive increments of uniform nonspecific cortical excitation. At $Q_{ns} = 1.2$ the system is just short of runaway self-excitation, which occurs when the mean values of $Q_e$ reach approximately 0.04.

It is seen that with progressive increase in $Q_{ns}$ total spectral power increases, and the peak spectral density moves to the right, toward a limiting case at which spectral power is distributed in the high beta to gamma range.

The top left hand graphs show these features of ECoG spectral behaviour for the complete model of the cat brain. The top right hand graphs were obtained with the matched linearised version. In the lower two sets of graphs, results when inhibitory to excitatory couplings, $\{\beta_{ie}\}$, are set to zero, and intracortical excitatory couplings, $\{\beta_{ee}\}$, are set to zero, are respectively shown.

It is seen that the complete (nonlinear) and linearised results are little different. With the removal of excitatory/inhibitory interactions the shift of peak spectral density to the right does not take place with increasing $Q_{ns}$,

[1]Here, as in earlier papers, the term zero bounds implies that axonal transmissions disappear at the boundary - equivalently, the boundary is absorbing.

and with the removal of $\beta_{ee}$ couplings, spectral behaviours are similar to those of the complete model, but of diminished amplitude.

Not shown in Figure 1 are the results of removals of $\beta_{ii}$-type and $\alpha$ - type couplings. The first of these cases ($\{\beta_{ii}\} = 0$) gives spectral results resembling the complete model, but with a small relative increase of peak power best seen in the $Q_{ns} = 1.2$ case. The second case ($\{\alpha_{ee}\} = 0$) is of course the case for the isolated unit volume, and no wave propagation in the matrix is possible.

In addition to simulation runs with synchronous noise inputs to column zero, runs were performed with sinusoidal $Q_s$ inputs (single sinusoids and combinations, across the frequency spectrum of interest) and asynchronous (uncorrelated) $Q_s$ noise drives to each unit volume in column zero. Asynchrony of the inputs lowered ECoG output amplitude without affecting spectral density. Sinusoidal inputs, single or in combination yielded output ECoG in which almost all spectral power was concentrated at the input frequency(s), with components several orders of magnitude lower, at integer multiples and fractions of the input frequency.

Figure 1 describes ensemble averages. Since real ECoG is usually spectrally characterised over short epochs, Figure 2 shows a set of examples of 0.8s spectra. It is seen that random fluctuations in the spectra of the input noise, and the transfer function of the cortical medium under the control of $Q_{ns}$, respectively control the transient fine spectral structure, and the form of the spectral envelope. Both the transient examples, and the ensemble averages appear similar to typical equivalent spectra from real ECoG, as seen in our laboratory and elsewhere.

*3.2. Effects of nonuniform excitation.*

*3.2.1. Zero-lag cross-correlation and ECoG gamma-band activity.*

Figures 3 show results obtained from the standard form of the simulation, when equal DC inputs ($Q_{ns}$), and asynchronous noise inputs of equal rms amplitude ($Q_s$) are delivered to two seperated unit volumes on the matrix - in these examples, to the (6,10) and (12,10) (row,columns).

In Figure 3a the $Q_{ns}$ input is of insufficient magnitude to elevate mean pulse density at the sites of input to the point where runaway self-excitation will supervene at the sites of driving - so the average pulse densities, $\{\bar{Q_e}\}$, at the driven sites remain low fractions. A surrounding field of secondarily excited unit volumes are revealed by the surface of pulse density variance.

The ECoG power spectrum from the middle of this field (the 10,10 site) is representative in spectral density of ECoG from all unit volumes, and resembles the spectra produced with low uniform $Q_{ns}$.

Cross-correlations of pulse densities from unit volumes of interest on the matrix show, from top down, that:

(i) pulse density fluctuation is essentially uncorrelated at the sites of input. (The inputs themselves had correlation of zero at all lags, and the correlations of the input sites were always low and maximal at variable lag)

(ii) pulse density at a driven site, and pulse density at any immediate neighbour to this site, are maximally correlated at a few msec. lag - ie, the neighbouring unit volumes are following the driven unit volume. This is shown for the (6,11) following the driven (6,10) site, but the result is general for all immediate neighbours.

(iii) pulse densities in immediate neighbours of each of the driven sites are maximally cross-correlated at zero lag. This result, shown for the (6,11) and (12,9) unit volume sites, is general between any pairs of neighbouring sites to the driven sites, and extends to the sites between the driving sites - eg site (10,10) has maximal cross-correlation at zero lag with neighbours of either driven site, as will be shown further below.

In Figure 3b cases are shown in which the $Q_{ns}$ inputs are similar to those in Figure 3a but the rms amplitude of the asynchronous driving noises is greater. The increase in noise magnitude is just such that pulse density at the driven sites fluctuates between the upper and lower bounds of $Q_e$. Average pulse densities remain lower than the maximum possible. In this condition pulse density cross-correlations follow the same general rules as in Figure 3a. However, the representative ECoG power spectrum shows high amplitude at low frequency, and a strongly hyperbolic form.

Figure 3c shows effects of higher $Q_{ns}$ inputs to the driven sites. The mean pulse density at the driven sites is now essentially at the maximum. The ECoG has moved to gamma band activity, centered around 40 Hz, and this spectrum is representative of activity throughout the matrix. Cross-correlations show the same general relations as in Figures 3a and b.

Results obtained in the form of Figures 3 were modified in the following ways in extended simulation runs, all using the standard model.

(a) When additional uncorrelated noise was injected to all other sites on the matrix, maximum cross-correlations declined, and ECoG spectra from remote unit volumes (eg, 0,0) exhibited typical low $Q_{ns}$ form, rather than simply following the spectra of unit volumes nearer the highly excited sites.

(b) When synchronous components were added to the asynchronous noises delivered to the driven sites, results were essentially similar, but maximum cross-correlations were higher.

(c) When the driven sites were moved further apart or closer together, then in the presence of additional noise, cross-correlation maxima were reduced with increasing distance of seperation of the input sites.

All cross-correlations reported above were calculated at 1 msec. lags. Lags as short as the step interval for the simulation (0.1msec) were also used, and it was shown that sites neighbouring each of the driven sites exhibited small perturbations of maximal cross-correlation about zero lag within short simulation runs, but had maxima at zero lag on average.

An attempt was made to determine the time of onset of zero-lag cross-correlation. Precise quantitaion is problematic because of the effects of simulation initialisation. But zero-lag cross-correlation appeared to be present within tens of milliseconds after initialisation.

Figures 4 show the extent of the domain of synchrony, its relation to the strength of average input to the driven sites, and the fact that synchrony is independent of the presence of gamma band ECoG oscillation. It can be seen that in both cases a central field of synchronously oscillating pulse density is surrounded by outwardly radiating travelling waves.Calculations from these lags indicate velocities are similar to those previously calculated for travelling waves.

*3.2.2 Mechanisms of synchrony and oscillation.*

*3.2.2.1 Oscillation: local phase relations of excitatory and inhibitory cells.*

As described with Figure 1, simulated gamma band ECoG oscillation is contingent upon the presence of local excitatory/inhibitory interactions. This is true also when $Q_s$ inputs are restricted to a pair of driven sites. To indicate the mechanism of this oscillation, Figure 5 shows the cross-correlations of the excitatory and inhibitory cells in a representative unit volume within the field of synchrony, in a simulation configuration identical to that applied to yield Figure 4.

As the level of excitation of the two driven unit volumes is increased to and beyond the point at which oscillation in the gamma range appears in the ECoG, excitatory and inhibitory pulse densities move toward an approximately quarter-cycle phase seperation, in terms of the principal period of oscillation.

*3.2.2.2. Synchrony: role of cortico-cortical ($\alpha_{ee}$) connections.*

Figures 6 were generated with a simulation configuration again like that used for Figure 4, and are again plotted for every unit volume with respect to the (10,10) site. The distribution of synchrony as a function of lag, and the values of positive correlation associated with the characteristic delays are shown.

Unlike the symmetric $\alpha_{ee}$-type couplings between unit volumes used in the generation of Figure 4, in these cases asymmetrical couplings ($E = 6$), were applied. It is seen that the pattern of delay is much transformed, but the central field of zero-lag synchrony, surrounded by outwardly radiating waves is preserved.

A closely similar pattern of delays and correlations is seen both in the upper and lower sets of graphs. Yet the lower figures were generated in simulation runs in which the model was linearised (on the basis of the mean values found in the equivalent complete model - see 2.4.1.) and both $\{\beta_{ee}\}$ and $\{\beta_{ie}\}$ were set to zero, thus eliminating both intracortical, local, excitatory/excitatory and excitatory/inhibitory interaction, and leaving only $\alpha$ - type, linear interactions in an asymetrically coupled matrix.

*3.2.3. Interneuronal, versus interareal, synchrony.*

Results presented so far use a simulation of a cat-sized brain, resolved to about 1 mm$^2$ unit volumes. As mentioned in 2.4.4, state equations of similar form can be used to represent interactions of individual neurones or small populations, so long as boundary conditions, coupling coefficients and delays are appropriately reconfigured.

Results with regard to synchrony at small scales are shown in Figure 7. These were obtained by:

(a) setting the boundary conditions of the matrix to zero (absorbing) bounds.

(b) setting $\{\alpha_{ee}\}$ to the usual value of $\{\beta_{ee}\}$, and $\{\beta_{ee}\}$ to zero, so that all excitatory couplings are intracortical and there is negligible self-excitation.

(c) setting the axonal conduction time for passage of signals across a single unit volume to zero, reflecting negligible local axonal delays.

(d) Again applying a highly asymmetric type of coupling between unit volumes, by use of the elliptical weighting of inputs, so as to better conform to the high asymmetry of synaptic couplings at microscopic scale.

(e) Raising the $Q_{ns}$ inputs to both the driven sites to a higher value ($Q_{ns} = 6$), and also the $Q_{ns}$ to other neurones/unit volumes to 0.5, so as

to increase (for numerical reasons) the dynamic gains to a degree sufficient to offset the fall in coupling strength when only intracortical couplings are modelled.

The simulation then represents to first approximation, a matrix of individual cells, or small populations of cells, connected together by intracortical fibres only.

It is seen in Figure 7 that synchronous activity appears at separated sites at this microscopic scale, as at the meso/macroscopic scales.

*3.2.4. Effect of total coupling gains upon synchrony.*

Figure 8 shows results again using a standard configuration with regard to couplings, axonal delay and boundary conditions. Here the input signals (high $Q_{ns}$ + asynchronous noise $Q_s$) has been applied not only to two discrete sites, but to four inputs sites, arranged in a bar. In this configuration couplings have are again rendered asymmetrical, by use of elliptical weighting of input couplings to unit volumes. This asymmetry has been arranged so that when the bar of inputs is applied to all sites from (7,10) to (13,10) it is acting on units which are relatively strongly coupled along the 10th row of the matrix. But when the bar is input diagonally, from sites (7,7) to (13,13) it is acting across relatively weakly coupled unit volumes. It is seen that the extent and amplitude of the field of synchronous activity is influenced by the orientation of the input.

These results depend essentially upon manipulating the gain of couplings between involved units. This can be acheived structurally, by manipulating symmetry of $\alpha$ -type couplings as shown, or by dynamic influences - ie, by manipulating the pattern of $Q_{ns}$ inputs.The latter, equivalent result to that shown for stuctural manipulation, follows from the fact that the total gain between any two unit volumes is a function of the structural terms $\alpha$ and $g$, and the dynamic gain term $dQ/dV$, which is in turn a function of $Q_{ns}$.

**4. Conclusions.**

*4.1 Summary of findings.*

It appears that both travelling EEG waves, and zero lag pulse synchrony and oscillation can be accounted for by a relatively simple system of state equations, even though these do not model most aspects of individual cell physiology in any detail.

Narrow bandwidth EEG activity - alpha activity in particular- is not fully accounted for, and must be taken to reflect rhythmic input to cortex

from subcortical sites, rather than arising in the cortex itself. Nonetheless the regulation of the cortical wave transfer function by nonspecific cortical excitation can account for much of the relative amplitude of EEG frequency components.

Synchronous oscillations in this simulation do not depend upon synchrony of inputs to seperated cortical sites, and are manifest at both microscopic and meso/macroscopic scales. The extent of the field of synchrony is regulated by the pattern of gains - both structural and dynamic - within the field of coupled elements.

*4.2 Mechanisms determining spectral form, synchrony and oscillation.*

Results described with Figure 1 enable consideration of ECoG spectral envelope as the sum of two essentially linear processes - one dependent on excitatory/inhibitory interactions, and one dependent on excitatory/excitatory interactions. From results in Figures 6 and 7, zero-lag synchrony depends upon linear excitatory couplings alone, and is robust despite asymmetry of couplings, and variation of axonal lag.

The basic mechanisms underlying the phenomena can be deduced as follows:

*4.2.1 Spectral envelope.*

As indicated in Figure 5, given a sufficiently excited state, excitatory/inhibitory interactions generate oscillation at a center frequency of about 40 Hz, in accord with the prediction of Freeman (1991). This process appears to give rise to one distinct component in the spectrum.

A second distinct spectral component may be accounted for as follows. Each unit volume is associated with a system of recurrent loops of cortico-cortical connections, leading back to the reference unit volume. If there are $n$ steps of one synapse in a particular recurrent loop, the mean delay in this loop is $\delta$ per synaptic step, and $\gamma$ is the mean gain at each step, then the recurrent loop's activity is associated with resonance at $f = 1/n\delta$ with a gain of $\gamma^n$. If each unit volume is connected to $\eta$ other unit volumes, then the number of recurrent loops of $n$ synaptic steps which can be formed is proportional to $\eta^n$, and the recurrent gain $G(f)$ of each excitatory mass upon itself is thus proportional to $\gamma^n * \eta^n$. Thus when $\eta = 1/\gamma$, $G(f)$ along pathways of any $n$ is (roughly) equal, the aggregate of self coupling, $\gamma * \eta = 1$, and the system is on the verge of runaway excitation. When $\eta \succ 1/\gamma, G(f)$ is monotonically descending with $f$ , and the system is stable. When $\eta \prec$

$1/\gamma$, $G(f)$ is monotonically ascending with $f$, and the system enters runaway self-excitation.[2]

The two components together appear to account for the forms of the spectral envelope, their sum dictating the frequency of peak power transfer from inputs.

The further spectral effect which appears when levels of pulse density vary rapidly from low to maximal action potential rates, as shown in Figure 3(b), may contribute to the typical "1/f " form seen in desynchonised real ECoG.

*4.2.2. Zero lag synchrony.*

The occurence and spatial conformation of synchrony in the simulation depends on long range excitatory couplings, gains and lags only, and is linear in nature. This property is not one commonly encountered in a linear wave medium. Notably there is not synchrony between the driven sites themselves, and both the neighbour sites, and activity beyond the field of synchrony exhibit lag correlations with input sites consistent with the propagation of travelling waves. Thus the synchronous field must be accounted for as a property of intersecting, weakly dispersive linear waves propagating from each input site. An analytic treatment of correlation functions in an equivalent continuum wave model is in preparation.

*4.3 Match to experimental results and other theoretical accounts.*

The simulation's qualitative behaviours correspond to the experimental phenomena reported in Singer and Gray's (1995) summary review of synchrony and oscillation results. They contrast with some of the explanations advanced by other writers. The mechanism of 40 Hz oscillation is closely akin to that proposed by Freeman (1991), but appears rather different to that modelled in hippocampus by Whittington et al (1995). Further there is no dependence upon subcortical rhythmic inputs (Llinas et al 1991: Steriade et al 1993), nor limit-cycle oscillations (Tass and Haken 1996), nor local lateral inhibition (Nischwitz and Glunder 1995), nor do the effects depend upon comparator properties of individual neurones (Konig et al 1996). However, these various alternate mechanisms may be complementary, or applicable in different situations, in ways which are not yet clear.

[2] A more rigorous development of this arguement depends upon assumptions concerning the distribution of long-range couplings, but the general conclusion regarding the spectral behaviour is robust.

The Singer and Gray (1995) findings can be considered accounted for to the following extent:

(a) Synchrony at exactly zero lag appears over the correct time course, and is present at all neural scales from individual neurones within a column, to interareal extents. Roles for both structural connectivity gains, and functional gain are provided, which concur with the interpretations given to their findings by Singer and Gray (1995).

(b) Synchrony is not contingent upon the presence of gamma band oscillation. Singer and Gray emphasise the seperability of these phenomena in experimental situations, although experimentally they are likely to appear together, when stimulus conditions are strong and nonspecific activation high.

(c) Synchrony is not present between the cells receiving input, but in those surrounding the sites of input. This may explain why synchrony is best observed as a multiunit phenomenon.

(d) The neighbouring sites to input actually follow the input sites with a few milliseconds lag. If it is assumed that cortical neurones which are optimally driven by visual stimuli correspond to those more directly receiving sensory input, while those suboptimally driven by sensory input are more strongly coupled to, and following, the neurones at the sites of direct input, then an explanation of why optimally driven neurones phase-lead those suboptimally driven (Konig et al 1995) is apparent. Yet the density of local connection would involve the both types in synchronous oscillation to some extent.

(e) When visual inputs which produce synchrony in response to short bars are concurrently stimulated with a large bar which links the stimuli delivered to the two sites, synchronous oscillation is enhanced (Singer and Gray 1995). This may be accounted for by the influence of the longer bar upon functional gains in the field of synchrony. However, a detailed explanation would need to allow for the influences of overlying noise, etc, which have not been modelled in any detail.

(f) Dependence of synchrony on subtle aspects of sensory tuning (eg, to movement and spatial frequency) has not been accounted for in these simulations. These findings do not constitute evidence against the general validity of this model, but pose a challenge for further detailed modelling. As in Singer and Gray's interpretation of their data, both structural and dynamic aspects of inter-unit gain must be considered to account for, eg, units resonding to stimuli of similar orientation.

(g) While reproduction of the experimental findings in simulations adds

little to debates concerning the relationship of synchrony and oscillation to cortical information processing, it should help to define a test-bed for modelling of the cognitive events. The field of synchrony contains information derived from both sites of asynchronous input. Given appropriate local synaptic modification (learning) rules, local networks could subsequently identify partial inputs as belonging to particular classes of associated spatio-temporal events. Also, the extended field of synchronous oscillation suggests that this mechanism may be important in ensuring redundancy of storage.[3]

(h) The simulation's properties imply that future experimentation might compare results at the intracortical, micro-level with macroscopic EEG waves in the surrounding field, and that events at these very different scales may yet share certain scale-invariant dynamics.

*4.4 Some general modelling aspects and limitations.*

Very simplified state equations compared to those used in most neuronal modelling nevertheless appear to have considerable explanatory power with regards to the dynamics of the neuronal field. It remains to be emphasised in which ways the simulation is restricted, and which aspects of the parameterisation appear critical.

Firstly, without the approximation to dendritic time constants which accord with the experimental findings of Freeman (but which are shorter than those commonly accepted) oscillation in the gamma band would not appear, since the period of oscillation is four times the dendritic rise time. Similarly, wave velocities are partially dependent on the dendritic rise time, as well as the axonal conduction velocity.

Secondly, without setting synaptic gain to a high figure, this simulation cannot combine both the range of spectral densities exhibited, and the low overall average pulse rate actually present in the neocortex (Amit et al 1990). Consequently the model readily enters runaway excitation. There is reason to believe that real neocortex may exploit such a metastability (Wright and Liley 1996), but an account of dynamic stabilising mechanisms is lacking at this stage.

Thirdly, the present model is unable to adequately account for the complex relations of ECoG rms amplitude and spectral density commonly re-

[3] In concurrent work Amit and Brunel (in press) have shown that a neural network with many common features with the present simulation has physiologically realistic behaviour under Hebbian memory storage, and exhibits synchronous oscillation associated with low pulse densities.

vealed in real ECoG - instead, amplitude rises monotonically with shift of the spectral enveope to the right. As a corrollary, the present model does not deal adequately with pulse density variance as a function of mean pulse density.

Fourthly, the description of subcortical inputs and cortico-cortical connectivities remain crude, but are also subject to reasonably simple improvement.

**Acknowledgements:** This work was supported by the Ross Trust, of Melbourne, Australia. The author thanks Nick Hawthorn for technical contributions.

**References.**

Amit DJ, Evans MR, Abeles M (1990) Attractor neural networks with biological probe records. Network 1: 381-405.

Amit DJ, Brunel N (1996) Spike rate variability, correlations and working memory in recurrent networks of spiking neurons. J. Neurophysiology (submitted).

Arnoldi HR, Brauer W (1996) Synchronisation without oscillatory neurones. Biol. Cybern. 74: 209-223.

Braitenberg V, Schuz A (1991) Anatomy of the Cortex: Statistics and Geometry. Springer, Berlin.

Bressler SL, Freeman WJ (1980) Frequency analysis of olfactory system EEG in cat, rabbit, and rat. Electroenceph. clin. neurophysiol. 50: 19-24.

Burkitt G (1994) Steady-state visually evoked potentials and travelling waves. PhD Dissertation. Swinburne University of Technology, Melbourne Australia.

Eckhorn R, Bauer B, Jordon W, Brosch M, Kruse W, Munk M, Reitboeck HJ (1988) Coherent oscillation: a mechanism of feature linking in visual cortex? Biol. Cybern. 60: 121-130.

Eekman FH, Freeman WJ (1990) Asymmetric sigmoid nonlinearity in the rat olfactory system. Brain Res. 557: 13-21.

Freeman WJ(1975) Mass Action in the Nervous System. Academic Press, New York.

Freeman WJ (1990) On the problem of anomalous dispersion in chaoto-chaotic phase transitions in neural masses, and its significance for the management of perceptual information in brains. In: Haken H, Stadler M (eds) Synergetics of Cognition. Springer, Berlin.

Freeman WJ (1991) Predictions on neocortical dynamics derived from studies in paleocortex. In: Basar E, Bullock TH (eds) Induced Rhythms of

the Brain. Birkhauser, Basel.

Freeman WJ (1995) Societies of Brains. The Spinoza Lectures. Erlbaum, New Jersey.

Gevins AS, Schaffer RE, Doyle JC, Cuttilo BA, Tannehill RS, Bressler SL (1983) Shadows of thought: shifting lateralisation of human brain electrical patterns during a brief visuomotor task. Science 220: 97-99.

Grey CM, Singer W (1989) Stimulus-specific neuronal oscillations in orientation columns of cat visual cortex. Proc. Natn. Acad. Sci. 86: 1698-1702.

Grey CM, Konig P, Engel AK, Singer W (1989) Oscillatory responses in cat visual cortex exhibit intercolumnar synchronisation which reflects global stimulus properties. Nature 388: 334-337.

John ER, Shimokochi M, Bartlett F (1969) Neural readout from memory during generalisation. Science 164: 1534-1536.

Konig P, Engel AK, Roelfsema PR, Singer W (1995) How precise is neuronal synchronisation? Neural Computation 7: 469-485.

Konig P, Engel AK, Singer W. (1996) Integrator or coincidence detector? The role of the cortical neuron revisited. Trends in Neuroscience 19: 130-137.

Liley DTJ, Wright JJ (1994) Intracortical connectivity of pyramidal and stellate cells: estimates of synaptic densities and coupling symmetry. Network 5: 175-189.

Llinas RR, Grace AA, Yarom Y (1991) In vitro neurons in cortical layer 4 exhibit intrinsic oscillatory activity in the 10- to 50-Hz frequency range. Proc. Natl. Acad. Sci. USA 88: 897-901.

Lopes da Silva FH, Storm van Leeuwin W (1978) The cortical alpha rhythm in dog: the depth and surface profile of phase. In: Brazier MA, Petsche H (eds) Architectonics of the Cerebral Cortex. Raven, New York.

Marsaglia G, Zaman A (1987) Towards a universal random number generator. Florida State University Report: FSU-SCRI-87-50.

Mitzdorf U. (1988) Evoked potentials and their physiological causes: an access to delocalised cortical activity. In: Basar E (ed) Dynamics of Sensory and Cognitive Processing by the Brain. Springer, Berlin Heidelberg New York.

Nunez PL (1981) Electric Fields of the Brain. Oxford University Press.New York.

Nunez PL (1989) Generation of human EEG by a combination of long and short range neocortical interactions. Brain Topography 1: 199-215.

Nunez PL (1995) Neocortical Dynamics and Human EEG Rhythms. Oxford University Press, New York.

Nischwitz A, Glunder H (1995) Local lateral inhibition: a key to spike synchronisation? Biol. Cybern. 73: 389-400.

Picton TW, Hillyard SA (1988) Endogenous event related potentials. In: Picton TW (ed) EEG Handbook. Elsevier Amsterdam.

Singer W. (1994) Putative functions of temporal correlations in neocortical processing. In: Koch C. and Davis JL (eds) Large Scale Neuronal Theories of the Brain. MIT Press, Cambridge Mass., London.

Singer W., Gray CM. (1995) Visual feature integration and the temporal correlation hypothesis. Annu. Rev. Neurosci. 18: 555-586.

Steriade M, Gloor P, Llinas RR, Lopes da Silva FH, Messulam MM (1990) Basic mechanisms of cerebral rhythmic activities. Electroenceph. clin. neurophysiol. 76: 481-508.

Steriade M, Curro-Dossi R, Contreras D (1993) Electrophysiological properties of intralaminar thalamocortical cells discharging rhythmic (≈40 Hz) spike-bursts at ≈1000 Hz during waking and rapid eye movement sleep. Neuroscience 56: 1-9.

Tass P, Haken H. (1996) Synchronised oscillations in the visual cortex - a synergetic model. Biol. Cybern. 74: 31-39.

Thatcher RW, Krause PJ, Hrybyk M (1986) Cortico-cortical associations and EEG coherence: a two-compartmental model. Electroenceph. clin. neurophysiol. 64: 123-143.

Traub RD, Whittington MA, Stanford IM, Jeffereys JGR (1996) A mechanism for generation of long range synchronous fast oscillations in the cortex. Nature 383: 621-624.

Walter DO, Kado BS, Rhodes JM, Adey WR (1967) Electroencephalographic baselines in astronaut candidates estimated by computation and pattern recognition techniques. Aerospace Medicine 38: 371-379.

Whittington MA, Traub RD, Jefferys JGR (1995) Synchronised oscillations in interneuron networks driven by metabotropic glutamate receptor activation. Nature 373: 612-615.

Wright JJ (1990) Reticular activation and the dynamics of neuronal networks. Biol. Cybern. 62: 289-298.

Wright JJ, Sergejew AA (1991) Radial coherence, wave velocity and damping of electrocortical waves. Electroenceph. clin. neurophysiol. 79: 403-412.

Wright, JJ, Liley DTJ (1995) Simulation of electrocortical waves. Biol Cybern 72: 347-356.

Wright JJ, Liley DTJ (1996) Dynamics of the brain at global and microscopic scales: neural networks and the EEG. Behavioral and Brain Sciences.19: 285-320.

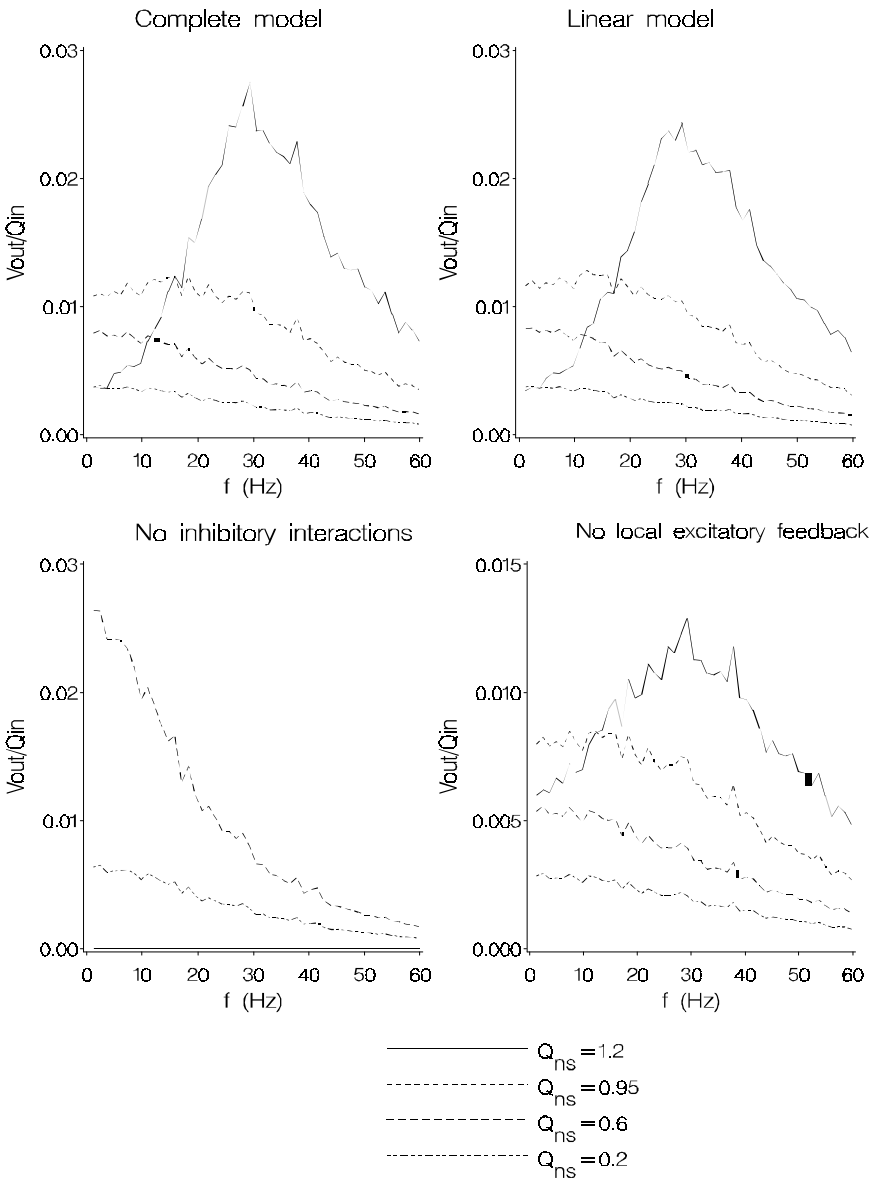


**Figure 1.**

Ensemble average properties of travelling waves in the simulation, obtained from driving the zeroeth column of the cortical matrix with synchronous white noise, Simulated electrocorticogram was obtained at site x = 10, y = 10. Gain is shown as a function of frequency, as the ratio of the ECoG amplitude, divided

by input pulse amplitude at column zero. Results are averaged from a hundred 0.8s epochs, each based on different driving noise seed value. Levels of nonspecific cortical activation ($Q_{ns}$) were increased to the maximum ($Q_{ns} = 1.2$) compatable with low pulse-density performance across the entire matrix.

Top left graph: Standard simulation, toroidal bounds, axonal delay 0.1msec/unit volume.

Top right: Matched performance when state equations are linearised about mean operating points of the standard simulation (see text).

Bottom left: Performance when the return couplings from inhibitory to excitatory cells are cut.

Bottom right: Performance when intracortical excitatory-excitatory couplings are cut.

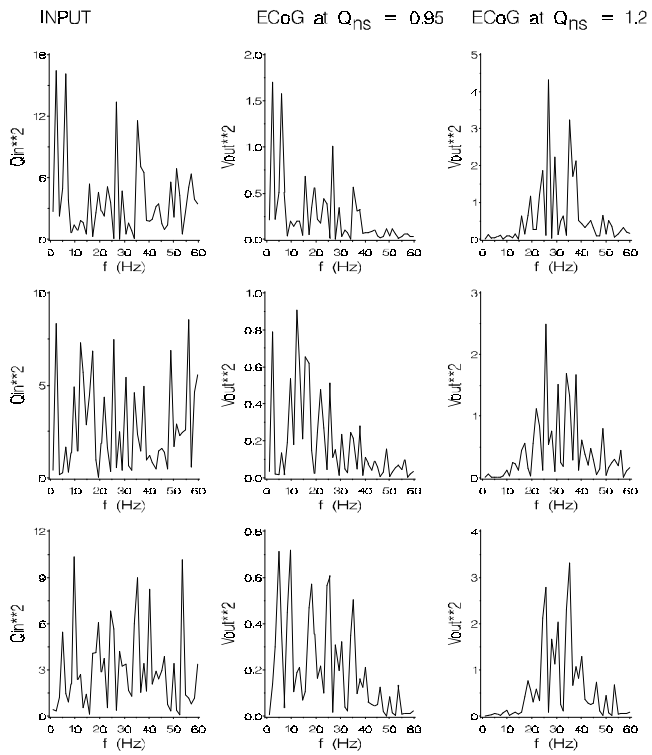


**Figure 2.**

Representative spectral properties of simulated ECoG output, and of the corresponding inputs, for randomly chosen 0.8s epochs, utilised in obtaining the ensemble average properties in Figure 1.

## Figures 3.

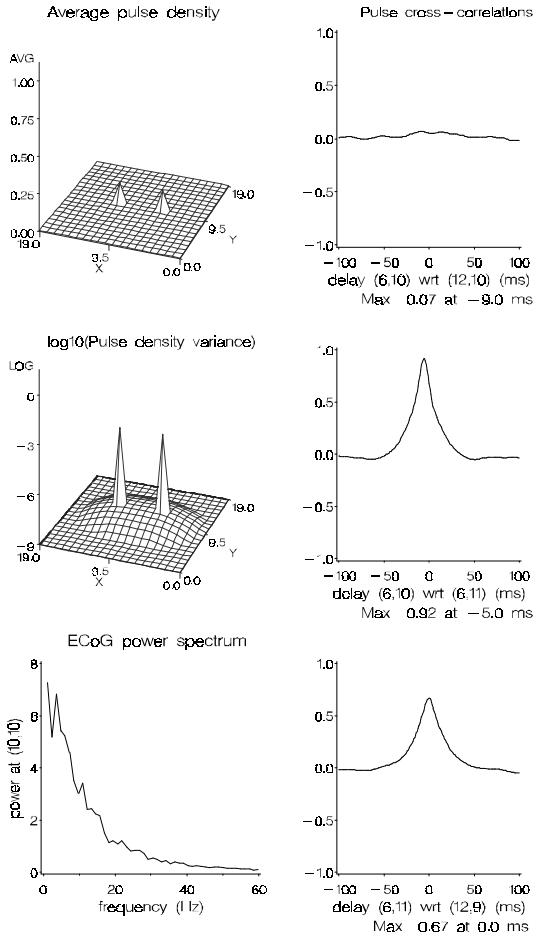


Each figure shows results when localised Qns input and asynchronous noise are delivered to sites x = 6, y = 10, and x = 12, y = 10, on the simulated cortical surface. Results averaged over 100 0.8s epochs.

Left columns of graphs: Average pulse density, and log variance of pulse density, on the cortical surface, with the average ECoG spectrum from x = 10, y = 10.

Right columns: Pulse cross-correlations in excitatory cell components, calculated at 1ms lags.

Top: Between the driven sites.

Middle: Between a driven site (x = 6, y = 10) with an immediate neighbour at (x = 6, y = 11).

Bottom : Between sites neighbouring the driven sites, at (6,11), and (12,9).

In all figures, the Qns input to all sites other than the driven sites was Qns = 0.1.

**Figure 3a.** Qns input to the driven sites = 4.84, and noise standard deviation (in units of Qe) = 0.0177.

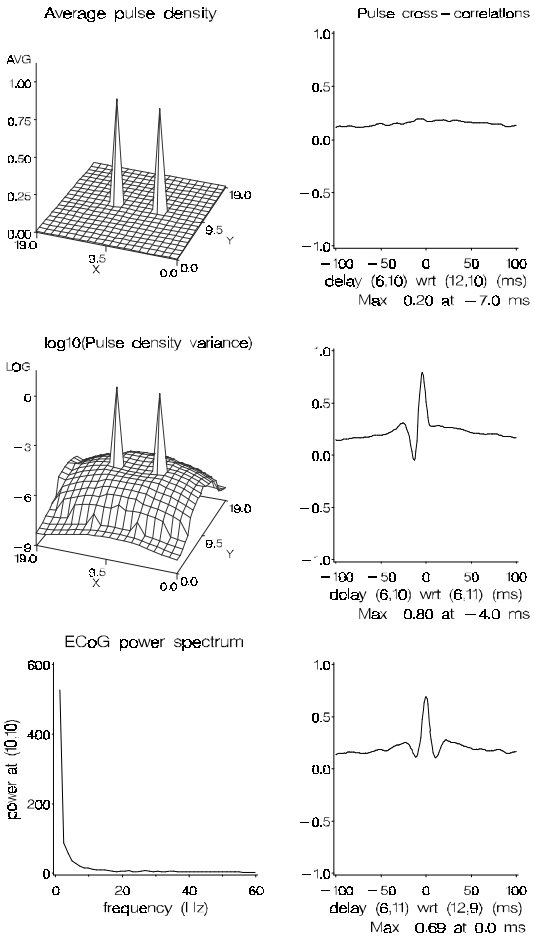


**Figure 3b.** Qns input to driven sites = 4.84, noise sd = 0.07

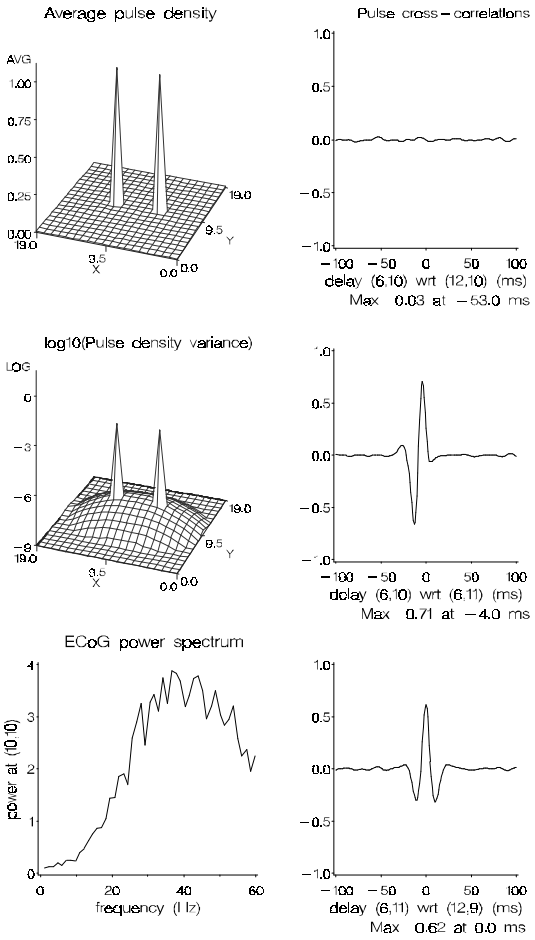


**Figure 3c.** Qns input to driven sites = 5.01, noise sd = 0.07.

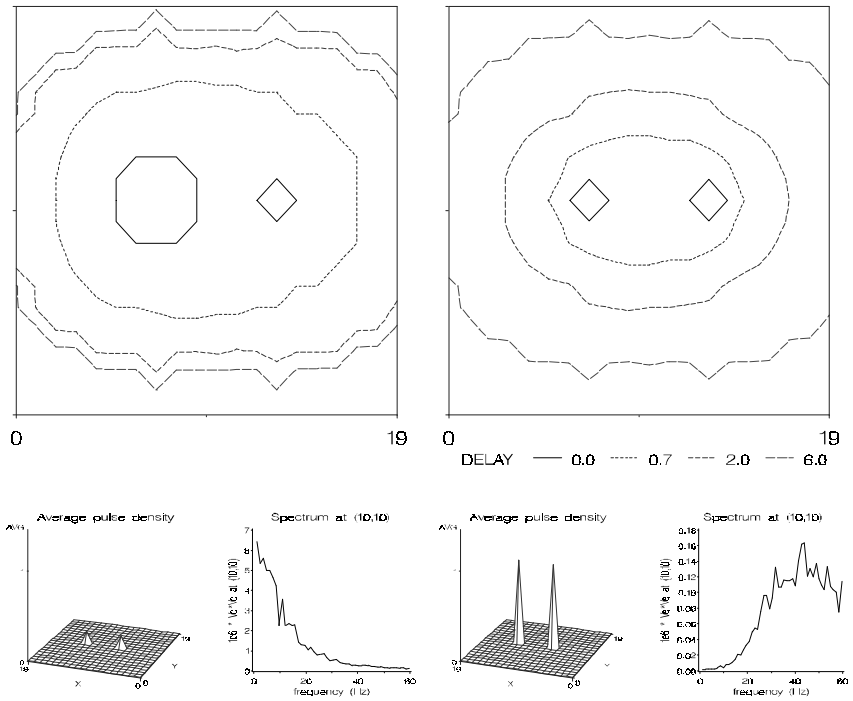


**Figure 4.**

The field of synchronous oscillation, and its surround of travelling waves.

Top figures. Surfaces corresponding to those shown in Figures 3a and c. In these instances inputs have been delivered to unit volumes at (7,10) and (13,10), so that the (10,10) site is centrally positioned in the field.

Left top surface: Delay of maximum positive cross-correlation of $Q_e$ between the (10,10) unit volume and all other unit volumes on the matrix. As for Figure 3a, the $Q_{ns}$ input to the two driven sites is 4.84.

Right top surface: Corresponding result when $Q_{ns}$ to the driven sites is 5.01, as in Figure 3c.

The small figures below each of these surfaces show the average value of $Q_e$ on the surface, and the ECoG spectrum arising from the (10,10) site.

Results here are ensemble averages from 50 independent initialisations of the simulation.

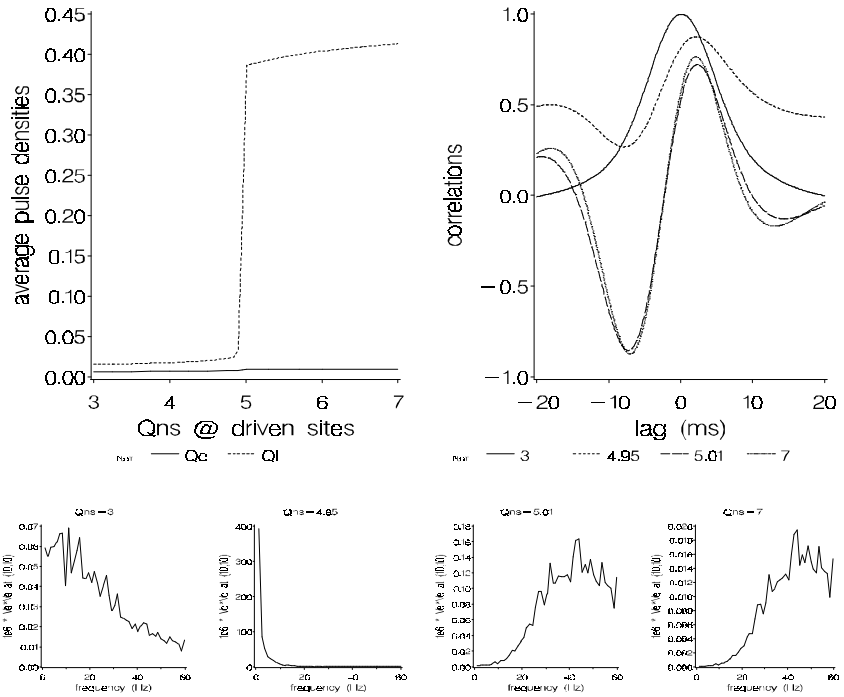


**Figure 5.**

Local excitatory/inhibitory pulse relations. Configuration of the simulation as in Figures 4. Mean pulse densities and cross-correlations within the (10,10) site.

Top left graph: Mean pulse density within the excitatory and inhibitory cell masses within the (10,10) unit volume, as $Q_{ns}$ increases at the driven sites at (7,10) and (13,10).

Top right graph: Cross-correlation of pulse density in the excitatory and inhibitory components, corresponding to the shifts in the means.

Bottom small graphs. Corresponding ECoG spectra at (10,10).

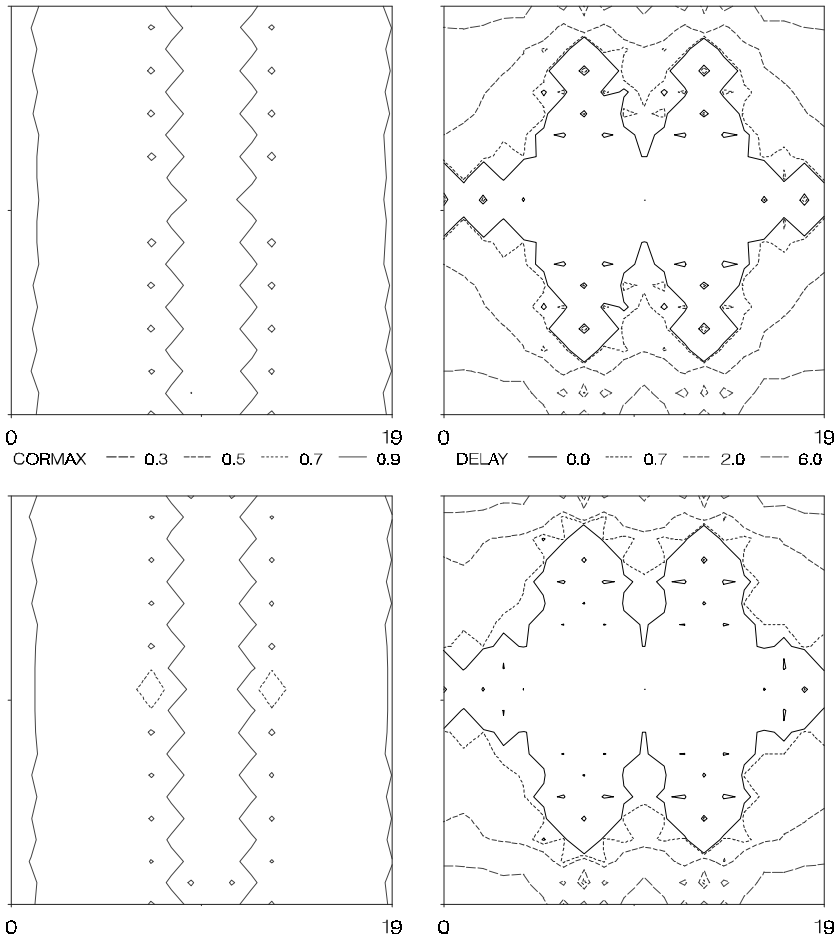


**Figure 6.**

These surfaces arise from simulation configurations, sites of noise input and $Q_{ns}$ input, analogous to Figure 4, and were formed over similar ensembles. In addition to mapping the lag time of peak positive cross-correlation wrt (10,10) - right hand surfaces - the correlation values associated with these lags are shown in the left hand surfaces.

Differences from Figures 4: The driven sites have a $Q_{ns}$ of 4.3, and instead of symmetrical couplings between unit volumes, couplings are asymetrical because of elliptical weighting of inputs to each unit volume. ($E = 6$, see sec.2.4.3).

Top surfaces. Complete non-linear model.

Bottom surfaces. Model linearised, and both intracortical connections and excitatory /inhibitory interactions abolished.

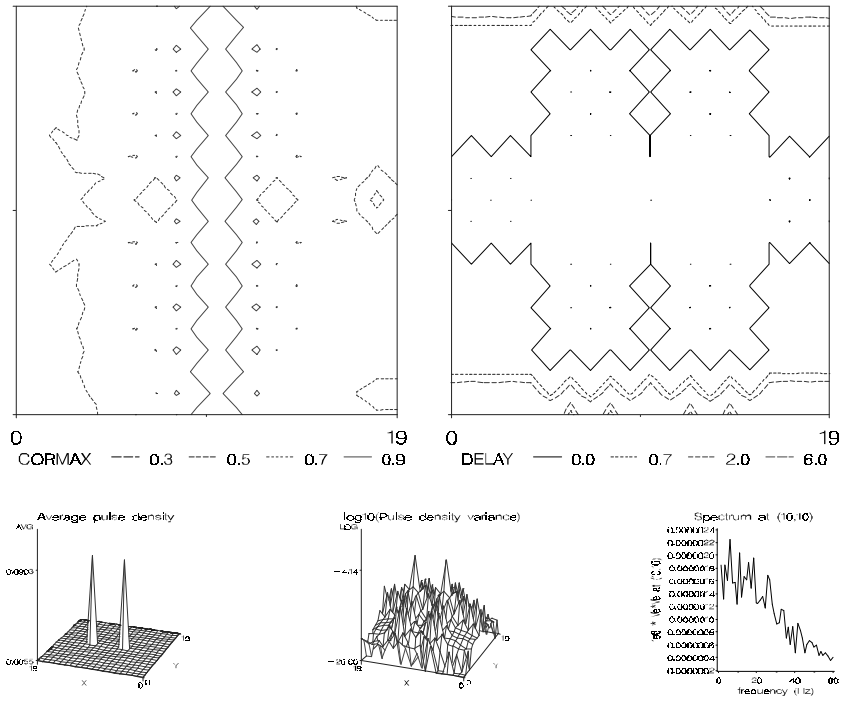


**Figure 7.**

Contours of maximal cross-correlation and delay with respect to the (10,10) site, when the coupling coefficient $\beta_{ee}$ is substituted for the cortico-cortical coupling coefficient $\alpha_{ee}$, axonal delays are set to zero, and boundary conditions are absorbing. Also $E = 6$, and $Q_{ns}$ values have been set to offset changes in aggregate gain (see text). Input sites remain at (7,10) and (13,10).

These changes approximate the simulation to the scale of average individual cells.

Top left surface - maximum cross-correlation,Top right surface - delay at maximum cross-correlation.

Bottom figures as labelled. Results are from the average of 25 individual runs.

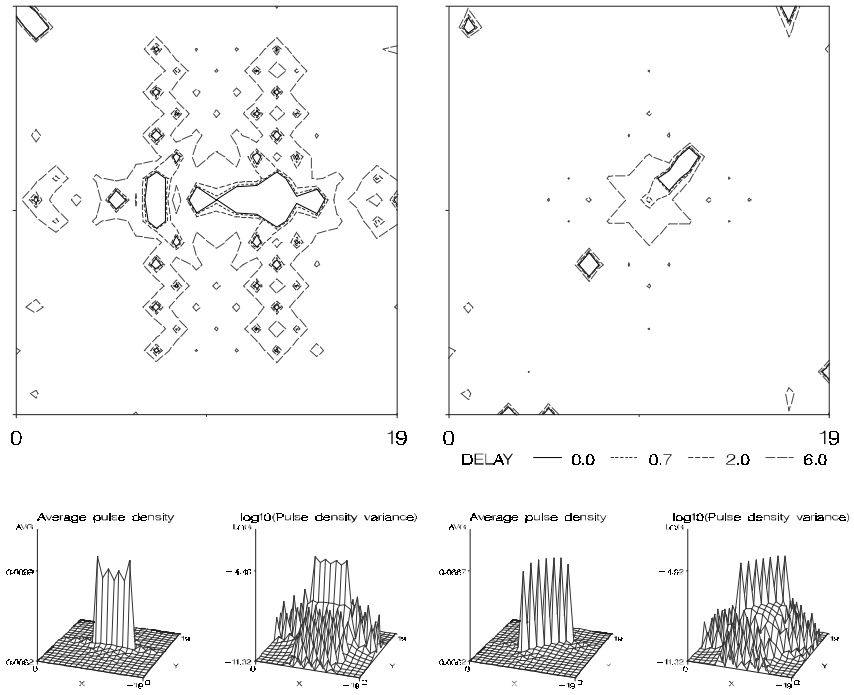


**Figure 8.**

Delay contours obtained when inputs to the simulation are delivered in conditions of asymmetric coupling, and the inputs are arranged in a continous bar, arrayed over the (7,10) to (13,10) sites, or the (7,7) to 13,13) sites. The value of elliptical weighting has been set to $E = 6$, with the consequence that the line of sites (7,10) to (13,10) is relatively strongly coupled, while the line of sites (7,7) to (13,13) is relatively weakly coupled. Asynchronous noise inputs were delivered to all sites on the bar, and a small amount of noise was input to all other sites to increase contrast.

$Q_{ns}$ to the driven sites is 3.8. Axonal delays etc. are otherwise standard, and the results are averaged from 25 individual runs.

Left hand graphs: Contours of maximum cross-correlation delay with respect to (10,10) and associated pulse densities and variance, for the bar stimulus over strongly coupled input sites.

Right hand graphs: Corresponding results for the weakly coupled input sites.

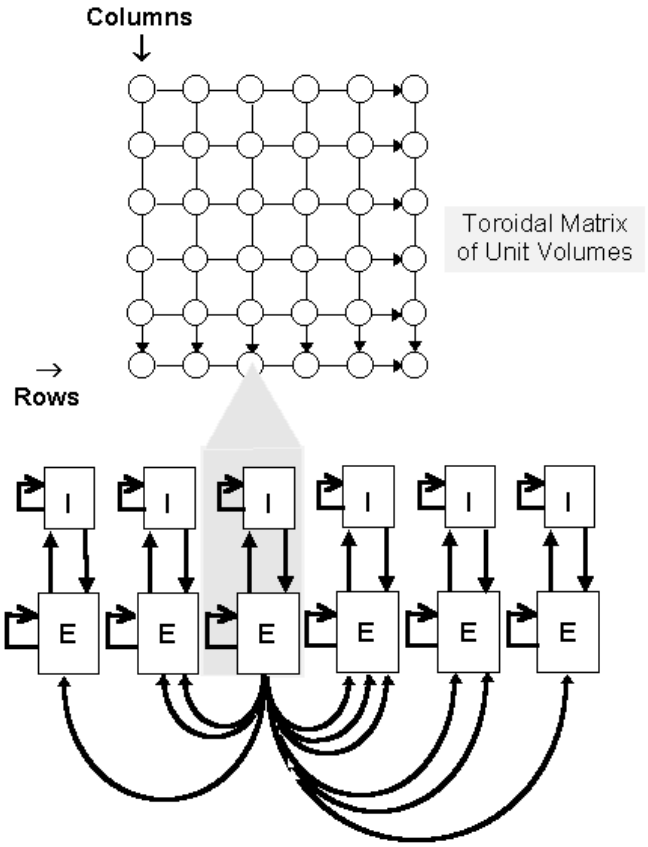


**Diagram 1.**

Schematic of connectivity in the simulation. Boxes labelled E, I, represent dendritic lag processes within each unit volume, shown shaded around a single unit volume. Solid arrows within a unit volume represent intracortical ($\beta$-type) axonal couplings with negligible delay, and coupling strength proportional to the density of synapses connecting the excitatory and inhibitory cells. Solid curves arrows represent cortico-cortical ($\alpha$-type) axonal couplings with lag proportional to distance, and coupling strength also proportional to synaptic density but diminishing as a Gaussian function with distance. Unit volumes are organised within a 20 X 20 matrix, and identified by row and column, from 0-19. The matrix is closed edge-to-edge by $\alpha$-type connections to creat a toroidal architecture.